Formamide Dimers: A Computational and Matrix Isolation Study

Artur Mardyukov,[†] Elsa Sánchez-Garcia,*,[†] Pawel Rodziewicz,[‡] Nikos L. Doltsinis,*,[‡,§] and Wolfram Sander*,[†]

Lehrstuhl für Organische Chemie II and Lehrstuhl für Theoretische Chemie,
Ruhr-Universität Bochum, D-44780 Bochum

Received: June 25, 2007; In Final Form: August 7, 2007

The dimerization of formamide (FMA) has been investigated by matrix isolation spectroscopy, static ab initio calculations, and ab initio molecular dynamics (AIMD) simulations. Comparison of the experimental matrix IR spectra with the ab initio calculations reveals that two types of dimers **A** and **C** are predominantly formed, with two and one strong NH···O hydrogen bonds, respectively. This is in accordance with previously published experiments. In addition, there is also experimental evidence for the formation of the thermally labile dimer **B** after deposition of high concentrations of FMA in solid xenon. The AIMD simulations of the aggregation process show that in all cases dimer **C** is initially formed, but rearrangement to the more stable doubly hydrogen-bonded structures **A** or **B** occurs for a fraction of collisions on the sub-picosecond time scale.

Introduction

Formamide (FMA) complexes provide simple models for the study of the intermolecular interactions in larger systems such as proteins or nucleic acids. The N−H···O=C and CH···O=C interactions in the formamide dimer and its double intermolecular proton transfer have been extensively studied by both theoretical and experimental methods.[1−12]

Vargas et al. identified five different FMA dimer structures as local minima using the Møller−Plesset second-order perturbation theory (MP2).[1] These structures were also studied by Frey and Leutwyler[10] using resolution of identity Møller−Plesset second-order perturbation theory (RIMP2) and the coupled cluster with singles, doubles, and perturbative triples (CCSD-(T)) method. Three structures called linear, zigzag, and cyclic dimers were studied by Bende et al. at the Hartree−Fock (HF) and MP2 levels of theory. They compared the results after using the a posteriori counterpoise (CP) method to correct for the basis set superposition error (BSSE) with the results of the a priori chemical Hamiltonian approach (CHA).[8]

Four FMA dimers were studied by Papamokos and Demetropoulos[9] in the assessment of the PW91XC functional with the 6-31+G* basis set for the vibrational spectra of amide dimers. Gómez Marigliano and Varetti calculated one cyclic and one "open" dimer of FMA with the B3LYP functional and 6-31G(d,p) or 6-31++G(d,p) basis sets as part of their experimental and quantum chemistry study of the self-association process of formamide in carbon tetrachloride solutions.[7] Grabowski et al. analyzed the N−H···O hydrogen bonds in the FMA dimer at the MP2/6-311++G(d,p) level of theory and applied the Bader theory to explain the nature of these interactions.[11] An ab initio molecular dynamics study of liquid FMA was reported by Tsuchida,[6] and Cabaleiro-Lago and Ríos developed an intermolecular potential function for interactions in FMA clusters based on ab initio calculations.[2]

FMA is strongly associated in the solid and liquid phases, as has been shown by vibrational spectroscopy.[13,14] IR investigations of the aggregation of FMA were carried out in chloroform[15] and in carbon tetrachloride.[7,15] The association of monomeric FMA in solid argon was studied by Räsänen using matrix isolation techniques.[5] Both an "open" structure with only one strong N−H···O hydrogen bond and a cyclic structure with two N−H···O hydrogen bonds are formed upon diffusion-controlled association in the matrix. In contrast, the dimers trapped from the gas phase consisted predominantly of the "open" structure. The dimers were characterized by analysis of the NH stretching and out-of-plane bending modes.

In the present paper, five minima of the FMA dimers **A**−**E** are found using the multiple minima hypersurface (MMH) approach[16−22] approach by exploring 1000 starting geometries generated without any previous chemical assumptions. Matrix isolation experiments are performed in argon and xenon matrixes, and the experimental IR spectra are compared to the results from static and dynamic ab initio calculations. Ab initio molecular dynamics (AIMD) simulations of the collision of two FMA monomers have been carried out. The experiments and calculations provide a detailed view of the aggregation process of formamide and allow the assignment of the IR spectra of individual formamide dimers.

Computational and Experimental Methods

Computational Methods. The MMH approach[16−22] was used for searching the minima of the FMA homo-dimers. One thousand randomly arranged FMA dimers were generated as starting points, and the resulting geometries were optimized and analyzed using PM3 and AM1[23−26] semiempirical quantum mechanical Hamiltonians. In this case, the PM3 and AM1 results do not totally agree, and most of the minima were found after refining the AM1 optimized geometries.

These semiempirical results provided a preliminary overview of the interactions in the FMA dimers, and the relevant configurations were further refined using second-order Møller−Plesset perturbation theory, MP2.[27] Pople's 6-31G(d,p) basis set[28,29] and cc-pVTZ, Dunning's correlation consistent triple ζ

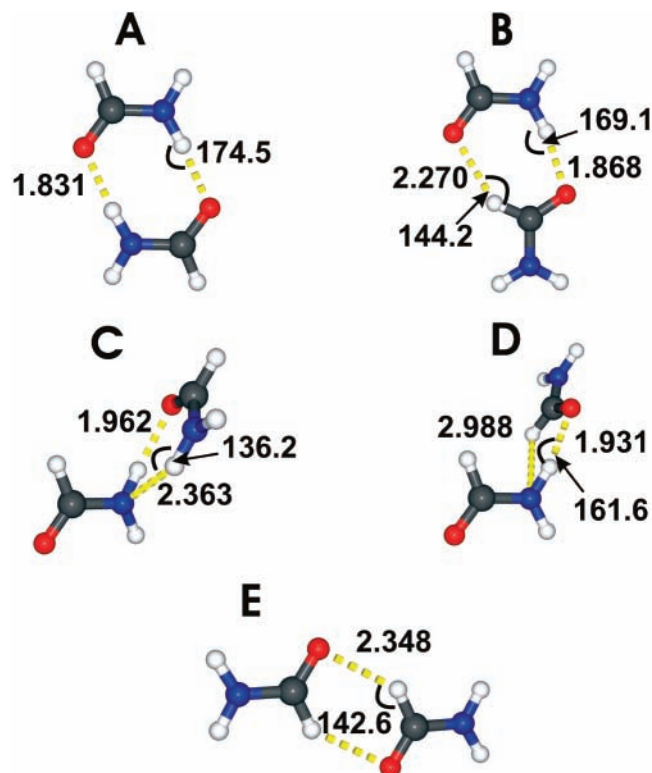Formamide Dimers

J. Phys. Chem. A, Vol. 111, No. 42, 2007 **10553**

Figure 1. Calculated structures with hydrogen bond lengths (Å) of the FMA dimers **A**−**E** at the MP2/cc-pVTZ level of theory.

TABLE 1: Calculated Binding Energies of the FMA Dimers A−E at the MP2/cc-pVTZ Basis Sets Including ZPE and BSSE Corrections Compared to the DFT/PBE Plane Wave (30 Ry Cutoff) Results[a]

	MP2/ cc-pVTZ				DFT/PBE pw
	ΔE	BSSE	ZPE	$\Delta E_{(BSSE+ZPE)}$	ΔE
A	−15.59	2.52	2.66	−10.41	−14.01
B	−10.66	2.06	2.06	−6.54	−9.12
C	−8.86	1.99	2.13	−4.74	−6.67
D	−7.82	1.70	1.75	−4.37	−8.03
E	−5.65	1.53	1.18	−2.94	−3.59

[a] All energies are given in kcal/mol.

basis set,[30] were used for tight geometry optimizations and calculation of the harmonic vibrational spectra.

The ab initio computations were performed using the Gaussian 98[31] and Gaussian 03[32] programs. The stabilization energies were calculated by subtracting the energies of the monomers from those of the complexes and including zero-point energy (ZPE) corrections. All of the energies were also corrected for the BSSEs using the CP scheme of Boys and Bernardi.[33]

Additional, both static and dynamic, calculations have been performed using the plane wave density functional code CPMD, version 3.10.[34] The Kohn−Sham equations were solved using the PBE exchange−correlation functional[35] in a plane wave basis set truncated at 30 Ry in conjunction with Vanderbilt ultrasoft pseudo-potentials.[36] Geometry optimizations were carried out employing screened periodic boundary conditions in an orthorhombic unit cell of size $14 \times 10 \times 10$ Å.[3] For the five most stable structures **A**−**E**, a Born−Oppenheimer molecular dynamics (BO-MD) simulation has been performed using a time step of 20 a.u. at a temperature of 100 K. The system was first equilibrated for 4 ps using a Nosé−Hoover chain thermostat[37] for each degree of freedom. In the production run of about 15 ps in length, a single Nosé−Hoover chain was used for the whole system to reproduce the canonical ensemble. Due to possible dynamical conformational changes of the system, a larger, cubic unit cell length of 14 Å has been used here. IR spectra have been computed for the BO-MD trajectories from the Fourier transform of the dipole moment autocorrelation function. The spectral assignment has been carried out using the effective normal-mode analysis tool by Martinez et al.[38]

In addition, a series of Car−Parrinello molecular dynamics (CP-MD) simulations has been performed to study the dimer formation process. These runs were carried out screening the periodic images at a temperature of 100 K using a time step of 4 a.u. and a fictitious electron mass of 400 a.u. A set of 20 initial configurations was picked at random from a high-

temperature CP-MD simulation at 300 K with fixed C atom positions where the two monomers rotated heavily. For each starting geometry two separate runs were performed following two different protocols. In the first protocol, the two formamide monomers were held at a fixed distance of 9.4 Å (measuring the C−C distance) in a $20.6 \times 10.6 \times 10.6$ Å^3 cell. A constrained run of at least 10 ps in length was carried out using a Nosé−Hoover chain for each degree of freedom keeping the positions of the C atoms fixed thus giving the two monomers a chance to align according to their dipole moments. In the subsequent 10−20 ps the constraint was released allowing the two monomers to collide. In this unconstrained period a single Nosé−Hoover chain was applied to the entire system. In the second protocol, the system was allowed to collide immediately during a 10 ps run without imposing any constraints thus reducing the extent of the previous alignment.

Matrix Isolation. Formamide was obtained from Aldrich (>99% purity), dried over molecular sieves (4 Å), and degassed several times by the freeze−pump−thaw method.[5] Matrix isolation experiments were performed by standard techniques using an APD CSW-202 Displex closed cycle helium refrigerator. Matrixes were produced by co-deposition of FMA with a large excess of argon (Messer Griesheim, 99.99%) or xenon (Messer Griesheim, 99.99%) on top of a cold CsI window with a rate of approximately 0.11 mmol/min. The FMA was evaporated from a glass tube kept at −30, −40, or −50 °C to control its vapor pressure. In a second set of experiments 600−800 mbar of argon or xenon were premixed with 0.5−1 mbar of FMA in a stainless steel flask. The flask was kept at 80 °C to avoid condensation of the FMA.

After deposition at 10 K the matrixes were annealed at higher temperatures either by keeping the matrix at a fixed temperature for several minutes or by warming with an approximate rate of 1 K/min. After the matrixes were cooled back to 10 K, spectra were recorded on a Bruker IFS spectrometer with 0.5 cm^{-1} resolution in the range between 400 and 4000 cm^{-1}.

Results

Calculated Geometries and Binding Energies. Five FMA homo-dimers **A**−**E** were localized at the MP2 level of theory with the cc-pVTZ basis set. The ZPE + BSSE corrected binding energies of the dimers are presented here. The geometries of these dimers agree very well with the complexes studied by Vargas et al.[1] and Frey and Leutwyler.[10] This shows, once again, the reliability of the MMH approach[16,17,19,20] for finding minima in hydrogen-bonded complexes without any previous chemical assumptions of the molecular geometries of the dimers, because all of our minima were found starting from completely randomly generated geometries.

There are four basic interactions in the FMA dimers:

(1) N−H···O interaction between the amide hydrogen atom of one FMA molecule and the carbonyl oxygen atom of the other FMA molecule.
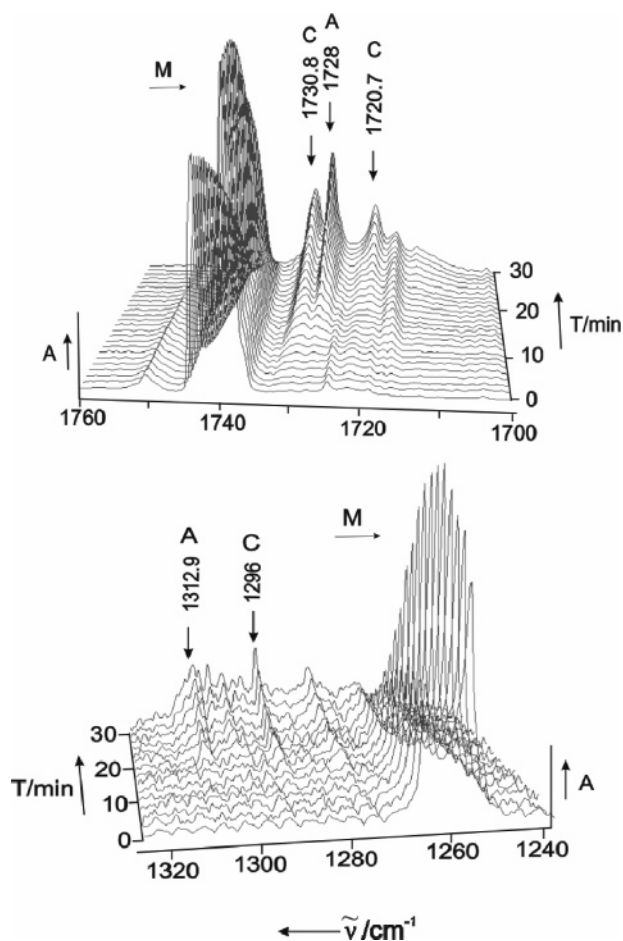
Figure 2. IR spectra of an argon matrix containing formamide during the slow warming from 10 K ($t = 0$ min) to 40 K ($t = 30$ min). Bands are assigned to monomeric formamide **M**, dimer **A**, and dimer **C**.

(2) CH···O interaction between the CH hydrogen atom of one FMA molecule and the carbonyl oxygen atom of the other FMA molecule.

(3) N−H···N interaction between the amide hydrogen atom of one FMA molecule and the nitrogen atom of the other FMA molecule.

(4) CH···N interaction between the CH hydrogen atom of one FMA molecule and the nitrogen atom of the other FMA molecule.

The most stable dimer **A** (-10.41 kcal/mol) is a cyclic C_{2h} complex stabilized exclusively by the N−H···O interaction 1 at 1.831 Å (Figure 1 and Table 1). The cyclic C_s dimer **B** (-6.54 kcal/mol) shows interaction 1 at 1.868 Å and interaction 2 at 2.270 Å hydrogen bond distances.

Dimers **C** (-4.74 kcal/mol) and **D** (-4.37 kcal/mol) show interesting structural similarities because they both stabilize due to interaction 1, and additionally, one FMA nitrogen atom is directly involved in a hydrogen bond. However, dimer **C** is additionally stabilized by interaction 3, whereas complex **D** shows the weaker interaction 4 (Figure 1 and Table 1).

The least stable FMA dimer is the cyclic C_{2h} complex **E** (-2.94 kcal/mol), which is stabilized exclusively by interaction 2. The differences in structure and binding energies of dimer **E** and dimers **A**, **B**, **C**, and **D** show the importance of the contribution of the amide groups to the stabilization of the FMA dimers. However, as the structure of dimer **E** demonstrates, interaction 2 plays an important role in defining the shape of the FMA complexes (Figure 1 and Table 1).

Table 1 also contains the dimer binding energies calculated

TABLE 2: Calculated and Experimental Vibrational Frequencies (cm^{-1}) of the FMA Monomer M

		monomer and factor of correction				
		argon		xenon		
mode	M calcd[a]	M expt	factor of correction	M expt	factor of correction	assignment
12	3787.1	3547.4	0.937	3536.7	0.933	$\nu_{as}(NH_2)$
11	3634.7	3426.6	0.943	3411.3	0.938	$\nu_s(NH_2)$
10	3017.2	2882.9	0.955	2851.4	0.945	ν (C−H)
9	1811.0	1739.1	0.960	1731.0	0.955	$\nu(C=O)$
8	1618.7	1575.8	0.973	1574.3	0.972	$\delta(NH_2)$
6	1285.0	1260.4	0.980	1267.2	0.986	$\nu(C−N)$
3	645.4	678.2	1.050	702.4	1.088	$\tau(NH_2)$

[a] Vibrational frequencies of the formamide monomer calculated at the MP2/cc-pVTZ level of theory.

using the density functional theory (DFT)/PBE method with a plane wave basis set truncated at 30 Ry. The DFT results have been obtained for DFT optimized geometries; they are seen to follow the same trend as the MP2 values except for the fact that the order of **C** and **D** is interchanged. At this point we should mention that the plane wave DFT calculations do not suffer from the BSSE, which may explain some of the minor deviations between the MP2 and the DFT results.

Matrix Isolation Experiments. The IR spectra of the FMA monomer **M** and the FMA dimers generated under various conditions of deposition and annealing of the matrixes were compared with spectra calculated at the MP2/cc-pVTZ level of theory (Tables 2 and 3). The formation of dimers and other molecular aggregates results in characteristic shifts of some of the vibrations of **M**. These shifts can be used to identify the dimers by comparison of the experimental and calculated data. To facilitate this comparison the calculated frequencies were scaled with individual factors to achieve for the monomer **M** an exact match of the calculated and experimental IR frequencies (**M**, Table 2; dimers **A**, **B**, and **C**, Table 3; dimers **D** and **E** calculated frequencies, Supporting Information).

The amount of monomer **M** and dimers formed in the matrix depends on (i) the partial pressure of FMA in the gas phase, (ii) the matrix temperature, and (iii) the matrix gas. (i) The partial pressure of FMA is controlled by the temperature of the FMA sample. At -50 °C the vapor pressure of FMA is very low, and mainly the monomer **M** is deposited in the matrix, whereas at -30 °C and higher temperatures the partial pressure of FMA is high enough to form dimers and other aggregates in the gas phase. These dimers are deposited in the matrix, and consequently, mixtures of **M** and dimers are found in the matrix. (ii) If matrixes (argon or xenon) are deposited on a spectroscopic window at 10 K, then the cooling process is very rapid, and the noble gases form crystals with many defects. Under these conditions the formation of aggregates during the deposition process is suppressed. (Only aggregates already formed in the gas phase are deposited.) If, however, the matrix is deposited at higher temperatures (30 K in argon or 50 K in xenon), then small molecules can diffuse during the deposition, and aggregates (in addition to those already present in the gas phase) are formed. Matrixes become "soft" (diffusion of small molecules becomes rapid) at approximately 30−50% of the melting point of the corresponding matrix gas. (iii) The experiments were performed in solid argon and xenon to elucidate the role of the matrix host on the formation of aggregates. In addition, due to the vapor pressure of the matrix gases, argon can only be annealed at temperatures below 40 K (at this temperature it sublimes rapidly off the matrix), whereas xenon matrixes can be warmed up to 70 K, which allows us to observe rearrange-

Formamide Dimers

J. Phys. Chem. A, Vol. 111, No. 42, 2007 **10555**

TABLE 3: Calculated and Experimental Vibrational Modes of the Formamide Dimers A, B, and C

MP2/cc-pVTZ (with Ar corrections)						argon matrix				MP2/cc-pVTZ (with Xe corrections)		xenon matrix		
A		B		C		A		C		A		A		
ν (cm^{-1})	I	ν (cm^{-1})	I	ν (cm^{-1})	I	ν (cm^{-1})	I	ν (cm^{-1})	I	ν (cm^{-1})	I	ν (cm^{-1})	I	assignment
3494.2	16	3544.7	10	3523.4	32	3515.1	13	3521.6	12	3479.2	16	3498.6	14	ν_{as} (NH$_2$)
		3498.6	16	3452.3	27									
3170.0	100	3424.2	9	3379.8	41	3130.6	10	3353.1	7	3153.1	100	3158.2	10	ν_s(NH$_2$)
		3193.3	100	3266.0	79			3219.1	3					
2902.0	19	2944.0	2	2912.3	24					2871.6	19	2863.6	2	ν(C–H)
		2879.5	20	2883.2	19									
1730.2	55	1729.8	95	1731.3	98	1728.0	100	1730.8	100	1721.2	55	1719.2	100	ν(C=O)
		1694.1	24	1714.4	100			1720.7	86					
1321.2	12	1312.3	15	1292.2	26	1312.9	11	1296.0	12	1329.3	12	1305.4	17	ν(C–N)
		1274.1	25	1256.4	32									
904.8	5	847.2	5	831.2	31	818.7	4	834.6	7	937.6	5	797.4	9	τ(NH$_2$)
		700.7	1	754.9	9			769.2	4					
										466.3^a	17	478.2	16	ω(NH$_2$)

^{a} Unscaled.

ments and reactions with slightly higher activation barriers. Specific interactions with the matrix guest, different sizes of matrix cavities, and different softening points and heats of sublimation contribute to the formation and stabilization of weakly interacting aggregates. The formation of a matrix is thus a complicated process, and from the formation or absence of aggregates in matrixes formed under the various conditions mentioned above only qualitative conclusions on the stabilities of dimers and other aggregates can be drawn.

Argon Matrix. The IR spectrum of monomer **M**, matrix-isolated in argon at 10 K, agrees very well with the spectrum reported in the literature.[5,12] The aggregation of FMA in inert gas matrixes was already studied by Räsänen.[5] They reported IR absorptions of two aggregates in the N–H stretching region and between 700 and 300 cm^{-1}. It was concluded that upon diffusion-controlled aggregation of **M** both "open" and cyclic dimers were formed in the matrix.

In our experiments the aggregation of **M** was induced by either warming the matrix (argon or xenon) from 10 to 40 K with a rate of approximately 1 K min^{-1} (free warming) or annealing the matrix at a defined temperature between 20 and 40 K for up to 60 min. In free warming experiments the intensity of the carbonyl stretching vibration of **M** at 1739.1 cm^{-1} starts to decrease at a temperature of 25 K, and simultaneously new bands at 1730.8, 1728.0, and 1720.7 cm^{-1} increase in intensity. At 25 K the band at 1728.0 cm^{-1} gains intensity faster than the bands at 1730.8 and 1720.7 cm^{-1}, indicating that two different species are formed. By comparison with ab initio calculations (MP2/cc-pVTZ) the band at 1728.0 cm^{-1} is assigned to the carbonyl vibration mode of dimer **A**, and the bands at 1730.8 and 1720.7 cm^{-1} are assigned to dimer **C** (Figures 2a and 2b and Table 3). Under both conditions, free warming and annealing of the matrix, mixtures of dimers **A** and **C** are formed. Dimer **A** corresponds to the cyclic dimer, and **C** to the "open" dimer described by Räsänen.[5]

As mentioned above, the C=O stretching vibration observed in argon at 10 K at 1728 cm^{-1} is in good agreement with the theoretical prediction (MP2/cc-pVTZ, scaled) for dimer **A** at 1730.2 cm^{-1}. Due to its symmetry, only one C=O stretching vibration is expected, whereas the other dimers with lower symmetry should exhibit two different C=O stretching vibrations. For dimer **B** these vibrations are predicted at 1729.8 (strong) and 1694.1 cm^{-1} (weak), and for dimer **C** at 1731.3 (strong) and 1714.4 cm^{-1} (strong). Thus, for dimer **B** one of the C=O stretch vibrations is calculated to be shifted more than

40 cm^{-1}, while for dimer **C** no shift larger than 25 cm^{-1} is predicted. Because in the experiment no new absorptions are found below 1710 cm^{-1} (Figure 2), we assign the second dimer observed in the matrix to dimer **C**. There is no evidence for the formation of dimer **B** as a major product in argon; however, we cannot exclude the formation of small amounts (<10%) of **B** if the predicted strong carbonyl stretching vibration overlaps with that of **A** or **C** and the weak absorption is below the detection limit.

The C–N stretching mode of monomer **M** is found at 1260.4 cm^{-1}. When the matrix is warmed, this band decreases in intensity, and bands at 1312.9 and 1296 cm^{-1} increase in intensity. The band at 1312.9 cm^{-1} is assigned to the C–N stretching vibration mode of dimer **A**, which is blue-shifted from the unperturbed molecule by 52.5 cm^{-1}. MP2/cc-pVTZ predicts a band at 1321.2 cm^{-1}, which is in reasonable agreement with the experimental value (Table 3). The band found at 1296 cm^{-1} is in good agreement with a vibration at 1292.2 cm^{-1} predicted for dimer **C**. For dimer **B** the corresponding vibrations are predicted to be at 1312.3 and 1274.1 cm^{-1}, respectively (Table 3).

As described by Räsänen,[5] annealing of a matrix containing **M** leads to new broad bands in the N–H stretching region (Figure 4 and Tables 3 and 4). Annealing results in a decrease of ν_{as}(NH$_2$) of **M** at 3547.4 cm^{-1} and the formation of an intense broad band at 3515.1 cm^{-1} and a less intense band at 3521.6 cm^{-1}. In agreement with the results of Räsänen,[5] the band at 3515.1 cm^{-1} is assigned to ν_{as}(NH$_2$) of **A** and the band at 3521.6 cm^{-1} to ν_{as}(NH$_2$) of **C** (Table 4).

In **M** ν_s(NH$_2$) is found at 3426.6 cm^{-1}, which after annealing is shifted to a set of broad bands in the range of 3450–3050 cm^{-1}. Although due to the broadness it is difficult to make clear assignments, some bands can be assigned to dimers **A** and **C**. The most intense band at 3130.6 cm^{-1} corresponds to **A**, and bands at 3353.1 and 3219.1 cm^{-1} to **C** (Table 3).

The NH$_2$ twisting vibration ω(NH$_2$) of **M** appears at 678.2 cm^{-1} (Figure 4). In **A** this vibration is shifted to 818.7 cm^{-1} (Table 4). Weak bands at 834.6 and 769.2 cm^{-1} correspond to dimer **C**, in excellent agreement with the predictions from ab initio calculations (831.2 and 754.9 cm^{-1}). Additional weak bands at 1717 and 1281 cm^{-1} are assigned to a FMA–H$_2$O complex formed by water contaminations in the matrix.[39] Comparison of the experimental spectra with spectra calculated for the dimers **D** and **E** did not give any evidence for the formation of these dimers (Table 3).
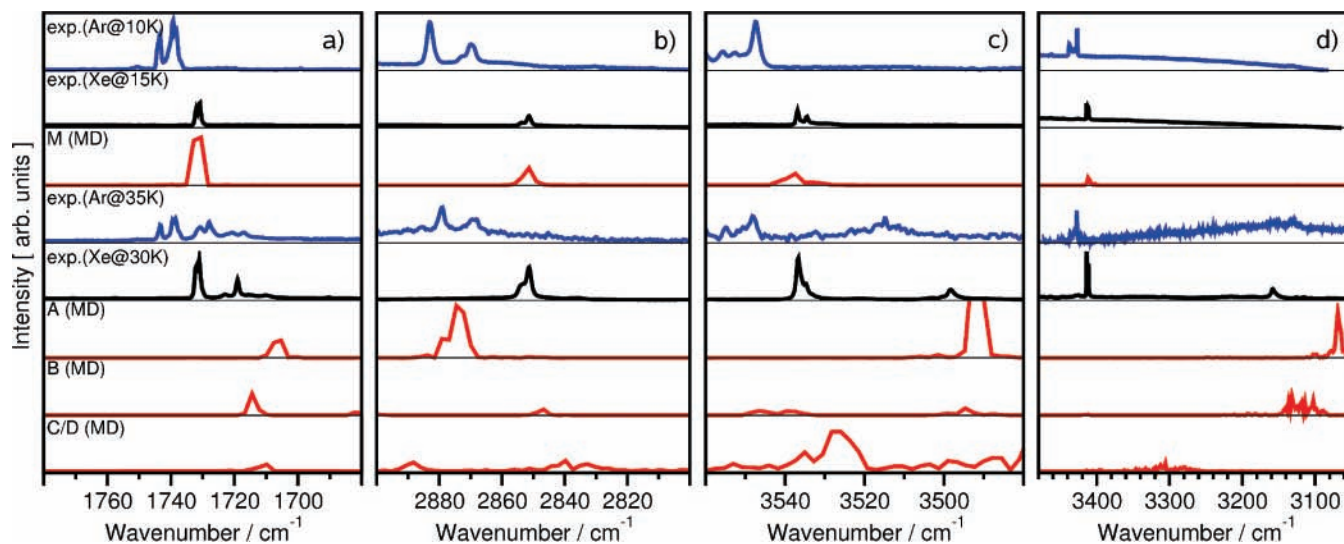
Figure 3. Experimental (Ar and Xe matrix isolation) and theoretical dynamical (DFT/PBE BO-MD simulations at 100 K) IR spectra of the FMA monomer **M** and the dimers **A**, **B**, and **C/D**. In the simulation labeled **C/D**, the system dynamically fluctuates between the **C** and the **D** local minima.
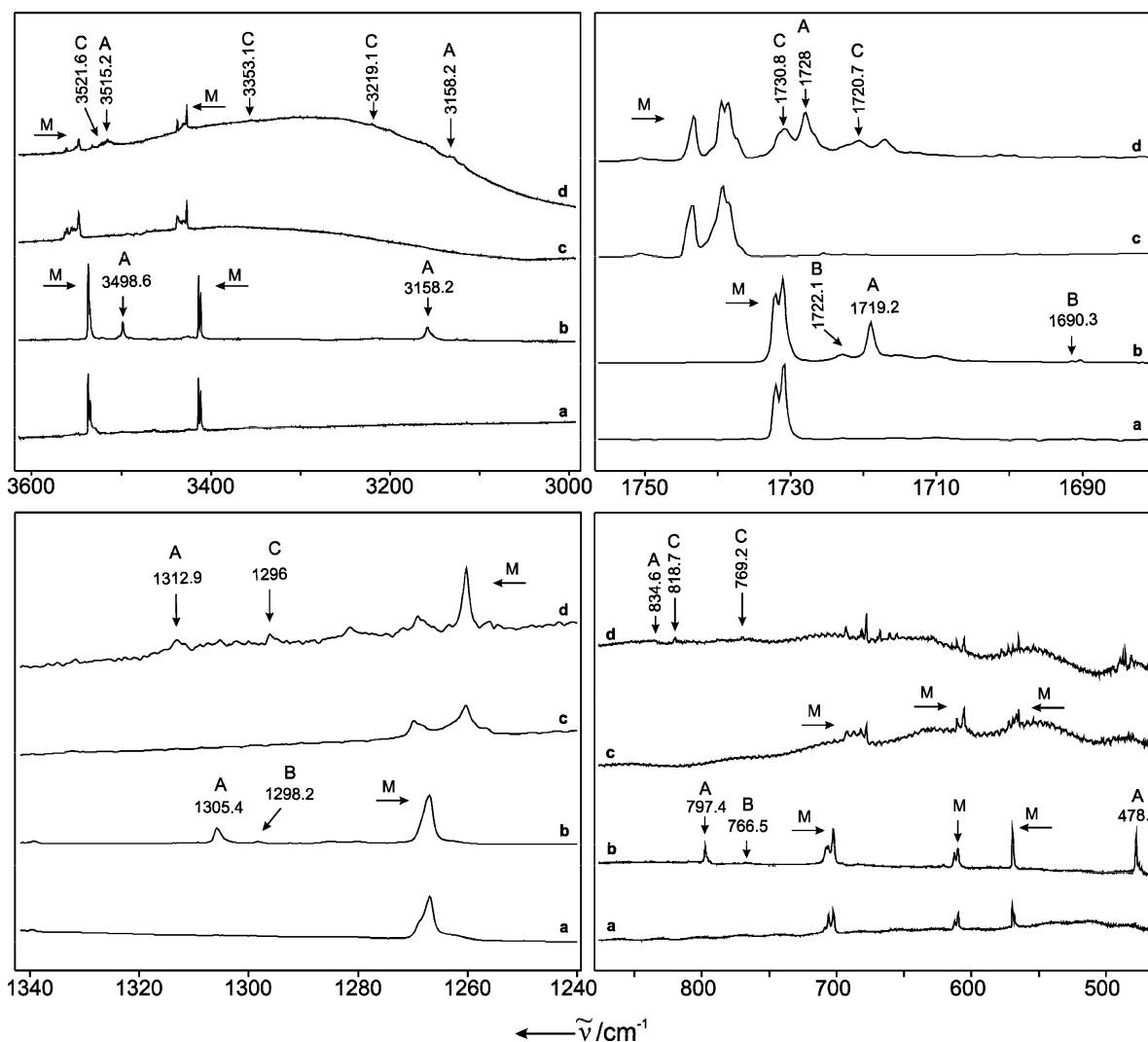

Figure 4. IR spectra of FMA in different sets of experiments. (a) Deposition of FMA at 15 K in xenon (sample temperature −50 °C). (b) Deposition of FMA at 30 K in xenon (sample temperature −30 °C). (c) Deposition of FMA at 10 K in argon (sample temperature −50 °C). (d) Changes after annealing at 35 K. Bands assigned to **M**, **A**, and **C** are labeled in the spectra.

Xenon Matrix. The spectrum of **M**, matrix-isolated in xenon, is in very good agreement with the spectra reported in the literature (Tables 2 and 3).[5,12] However, the composition of the matrixes very much depends on the sublimation temperature of FMA. Two types of experiments were performed: (i) FMA was sublimed from a sample kept at −50 °C and deposited with

Formamide Dimers

J. Phys. Chem. A, Vol. 111, No. 42, 2007 **10557**

TABLE 4: Vibrational Frequencies of the Normal Modes of Formamide Dimers Experimentally Found in This Work Compared to the Values from the Literature

argon matrix				xenon matrix		
A[a]	**A**[b]	**C**[a]	open dimer[b]	**A**[a]	**A**[b]	assignment
3515.1	3515	3521.6		3498.6	3510	$\nu_{as}(NH_2)$
3130.6	3216	3353.1	3369	3158.2	3158	$\nu_s(NH_2)$
	3195	3219.1	3355			
				2863.6		$\nu(C-H)$
1728.0		1730.8		1719.2		$\nu(C=O)$
		1720.7				
		1598.7				$\delta(NH_2)$
		1586.0				
1312.9		1296.0		1305.4		$\nu(C-N)$
818.7	819	834.6	769	797.4	797	$\tau(NH_2)$
		769.2				

[a] This Work. [b] Reference 5.

a large excess of xenon at a temperature of 15−30 K. Under these conditions, monomer **M** was found almost exclusively by IR spectroscopy (Figure 4). (ii) If FMA was sublimed at −30 °C, where its vapor pressure is considerably higher, then monomer **M** and additional bands assigned to dimers were found.

Annealing of a xenon matrix containing mainly **M** from 30 to 65 K results in the formation of sharp bands at 3498.6, 3158.2, 1719.2, 1305.4, 797.4, and 478.2 cm^{-1} showing identical kinetic behavior assigned to dimer **A**. This assignment was confirmed by comparison with the spectra obtained in argon and with results from MP2/cc-pVTZ calculations (Table 3). Except for the $\tau(NH_2)$ mode, the calculated vibrational modes are in good agreement with the experimental frequencies. The asymmetric NH$_2$ vibration of **A** appears as a sharp band at 3498.6 cm^{-1}, above 10 cm^{-1} from the band described by Räsänen.[5] (Table 4). However, the other bands assigned to **A** agree very well with the literature data. In addition, several very broad bands, presumably due to other aggregates, are observed that are difficult to assign.

If the xenon matrix is deposited at 30 K instead of 10 K and higher gas-phase concentrations of FMA are used (liquid FMA kept at −30 °C), then **M** and all bands assigned to **A** are found in the matrix even without annealing. Additional weak bands are observed at 1722.1, 1690.3, 1298.2, and 766.5 cm^{-1}. These additional bands proved to be labile and completely disappear during annealing at 50 K. Comparison with the results of MP2 calculations gives a reasonable agreement with the predicted spectrum of **B**. Thus, we tentatively assign the thermolabile compound to dimer **B**. Several other broad bands already formed after the deposition change shape and intensity during the annealing. Again, these bands could not be definitely assigned, although it is tempting to assume that **C** is formed as in the matrix. The broadness of these bands might result from the conformational flexibility of **C** and equilibria between **C** and **D**. Why **B** is detected in solid xenon but not (or only tentatively) in argon might be explained by subtle frequency shifts and line broadenings that result in overlapping bands making the detection difficult. In addition, matrix effects (size of the cavity etc.) might result in the stabilization of one or the other dimer. However, because matrix effects are difficult to quantify, they are not discussed here.

Simulated Dynamical IR Spectra. Before analysis of the dynamical finite temperature IR spectra obtained from BO-MD simulations, it is worth pointing out that there is good overall agreement between the harmonic vibrational frequencies obtained from static DFT/PBE calculations for the isolated formamide monomer and the dimers **A**, **B**, **C**, and **D** (Table 5)

and the MP2 results (Tables 2 and 3). We do not present any results for the dimer **E**, because it was found to be highly unstable and to dissociate in a molecular dynamics simulation. Table 6 contains the most important peak positions obtained by Fourier transformation of the dipole moment autocorrelation function from the BO-MD simulations at 100 K. Only selected vibrational modes that are important for assigning the experimental spectra are reported. We focused on the most characteristic spectroscopic evidence of dimer formation, namely, the C=O, C−H, symmetric NH$_2$, and asymmetric NH$_2$ vibrations.

Figure 3 shows a comparison of the calculated dynamical IR spectra of the monomer **M** and the dimers **A**, **B**, and **C/D** with the experimental spectra recorded in the Ar and the Xe matrix (see also Figure 4). In the case of Xe, the experimental spectra have been obtained from FMA deposition at 15 and 30 K, whereas for Ar FMA was deposited at 10 K and annealed to 35 K. For the intensities the same scale was used for all spectra obtained with a particular method; e.g., all theoretical spectra have the same intensity scale. In each panel of Figure 3 the theoretical frequencies have been scaled such that the respective monomer peak and the experimental peak measured in Xe at 15 K are aligned. This greatly facilitates the comparison and assignment of the spectra.

Comparison with IR Spectra in an Argon Matrix. The spectral region corresponding to the C=O stretching vibration (Figure 3a, Ar@35 K) exhibits three new peaks after annealing, red-shifted by 8, 11, and 18 cm^{-1} with respect to the monomer band. The simulation yields intense dimer bands (marked as strong in Table 6) that are red-shifted with respect to the monomer by 25, 16, and 21 cm^{-1} for dimers **A**, **B**, and **C/D,** respectively, which could explain the main experimental features in this region. However, the concentration of dimer **B** must be much smaller than that of dimer **A** or **C/D** because its theoretically predicted strongly red-shifted (by −48 cm^{-1}) weak band at 1682 cm^{-1} is below the detection limit in the experiment.

The C−H stretching vibration band is only weakly affected by the dimerization; the very broad band (Figure 3b) makes assignment difficult. There appear both red-shifted and blue-shifted features at 35 K, allowing, in principle, the assignment to all three dimer species, **A**, **B**, and **C/D**.

Figures 3c and 3d show the asymmetric and symmetric NH$_2$ stretching regions. In both cases the strongly red-shifted sharp spectral features could be attributed to dimers **A** or **B**, whereas the broad red-shifted features in the Ar matrix spectrum at 35 K may have been caused by dimer **C/D**. Thus, the comparison of the theoretical dynamical spectra with the experimental measurements in an argon matrix suggests that all three dimer species **A**, **B**, and **C/D** could be present in experiment, although there is only evidence for dimers **A** and **C**. Dimer **B** might be a minor constituent beyond the detection limit.

Comparison with IR Spectra in a Xenon Matrix. The experimental spectrum in a xenon matrix differs considerably from that reported for the argon matrix. We would like to emphasize that in the spectral region between 1680 and 1780 cm^{-1}, which includes the C=O stretching vibration, no frequency scaling of the theoretical data was necessary, as the simulated spectrum of **M** matches almost perfectly the experimental spectrum in Xe at 15 K (Figure 3a). The additional experimental bands at 1722, 1719, and 1690 cm^{-1} appearing in Xe at 30 K can be attributed to dimer formation. The relatively weak strongly red-shifted peak at 1690 cm^{-1} agrees well with the low-intensity C=O band at 1682 cm^{-1} of the theoretical spectrum of dimer **B**, while the prominent experimental feature at 1719 cm^{-1} and its side peaks could at this

TABLE 5: DFT/PBE Static (0 K) Harmonic Vibrational Frequencies (cm⁻¹) of the FMA Monomer M and the Dimers A, B, C and D[a]

M	A		B		C		D		assignment
3614 [38]	3559 [146]	(−55)	3613 [46]	(−1)	3597 [98]	(−17)	3610 [50]	(−4)	$\nu_{as}(NH_2)$
			3562 [68]	(−52)	3526 [76]	(−88)	3544 [109]	(−70)	
			3469 [30]	(0)	3437 [126]	(−32)	3471 [41]	(+2)	$\nu_s(NH_2)$
3469 [25]	3188 [1602]	(−281)	3145 [723]	(−324)	3264 [378]	(−205)	3295 [606]	(−174)	$\nu(C-H)$
2832 [110]	2852 [370]	(+20)	2885 [25]	(+53)	2873 [113]	(+41)	2867 [65]	(+35)	
			2830 [165]	(−2)	2827 [93]	(−5)	2822 [120]	(−10)	
1732 [412]	1707 [811]	(−25)	1713 [662]	(−19)	1721 [448]	(−11)	1718 [193]	(−14)	$\nu(C=O)$
			1675 [144]	(−57)	1701 [418]	(−31)	1705 [842]	(−27)	
			1578 [23]	(+26)	1578 [46]	(+26)	1578 [41]	(+26)	$\delta(NH_2)$
1552 [59]	1568 [23]	(+16)	1555 [39]	(+3)	1557 [26]	(+5)	1564 [46]	(+12)	
			1281 [85]	(+54)	1254 [85]	(+27)	1254 [71]	(+27)	$\nu(C-N)$
1227 [90]	1291 [147]	(+64)	1241 [150]	(+14)	1232 [108]	(+5)	1244 [103]	(+17)	
			814 [42]	(+185)	778 [115]	(+149)	765 [19]	(+136)	$\tau(NH_2)$
629 [14]	833 [78]	(+204)	647 [13]	(+18)	673 [36]	(+44)	645 [15]	(+16)	

[a] The values in square brackets are absolute intensities, and those in parentheses are frequency shifts relative to the monomer.

TABLE 6: DFT/PBE Dynamic (100 K) Unscaled Vibrational Frequencies (cm⁻¹) and Relative Intensities of the FMA Monomer M and the Dimers A, B, and C/D[a]

M	A		B		C/D		expt argon matrix	expt xenon matrix	assignment
3612vw	3567 m	(−45)	3617vw	(+5)	3602 m	(−10)	(−25.8)	(−38.1)	$\nu_{as}(NH_2)$
			3569vw	(−43)	3552 m	(−60)	(−32.3)		
3472w	3123s	(−349)	3476vw	(+4)	3456w	(−16)	(−73.5)	(−253.1)	$\nu_s(NH_2)$
			3186s	(−286)	3364s	(−108)	(−207.5)		
							(−296.0)		
2836w	2859s	(+23)	2891w	(+55)	2873 m	(+37)	-	(+12.2)	$\nu(C-H)$
			2831 m	(−5)	2824s	(−12)			
1730s	1705s	(−25)	1714s	(−16)	1709s	(−21)	(−8.3)	(−11.8)	$\nu(C=O)$
			1682w	(−48)	1721vw	(−9)	(−11.1)		
							(−18.4)		
1551w	1586w	(+35)	1574w	(+23)	1572w	(+21)	(+22.9)		$\delta(NH_2)$
			1558 m	(+7)	1558 m	(+7)	(+10.2)		
1218w	1289w	(+71)	1277 m	(+59)	1275w	(+57)	(+52.5)	(+38.2)	$\nu(C-N)$
			1236w	(+18)	1243s	(+25)	(+35.6)		
625vw	846w	(+221)	790w	(+165)			(+140.5)	(+95)	$\tau(NH_2)$
			641vw	(+16)			(+156.4)		
							(+91.0)		

[a] Experimental values for selected spectral regions are given for comparison. The values in parentheses are calculated frequency shifts with respect to the monomer. Description of the relative intensity of the bands reported: s, strong; m, medium; w, weak; vw, very weak.

point be composed of the dimers **A**, **B**, and **C/D**. However, after annealing to 60 K the experimental band at 1682 cm⁻¹ attributed to the complex **B** vanishes completely, whereas the other spectral features remain mostly unchanged. This shows that the sharp experimental peak at 1719 cm⁻¹ must be due to dimer **A**; complex **B** has rearranged into the thermodynamically most stable chemical dimer **A** species.

In the C−H region between 2800 and 2900 cm⁻¹ depicted in Figure 3b, the simulated dimer spectra show larger differences among each other, possibly helping assignment. Because in this vibrational domain the experimental spectrum changes little after annealing, our discussion holds in the temperature range from 30 to 60 K. Dimer **A** exhibits a moderate blue shift compared to **M**, whereas the positions of the most intense peaks of the

dimers **B** and **C/D** are slightly red-shifted. Dimer **C/D** also exhibits a blue-shifted feature, however its intensity being much lower than the dimer **A** band (see also Table 6). Because there is an indication of a blue-shifted feature in the experimental spectra it would seem that dimer **A** is present in experiment. The theoretical spectrum of dimer **B**, however, is nearly unshifted relative to **M** and could therefore be buried in the main spectral feature (Figure 3b). As expected due its floppiness, the spectrum of dimer **C/D** shows a pronounced broadening. Besides a new red-shifted feature there remains a significant contribution at the monomer position.

In the asymmetric NH₂ stretching region (Figure 3c), the experimental red shift of 38 cm⁻¹ might be assigned to the bands of dimers **A** and **B**, which are red-shifted by 45 and 43 cm⁻¹,
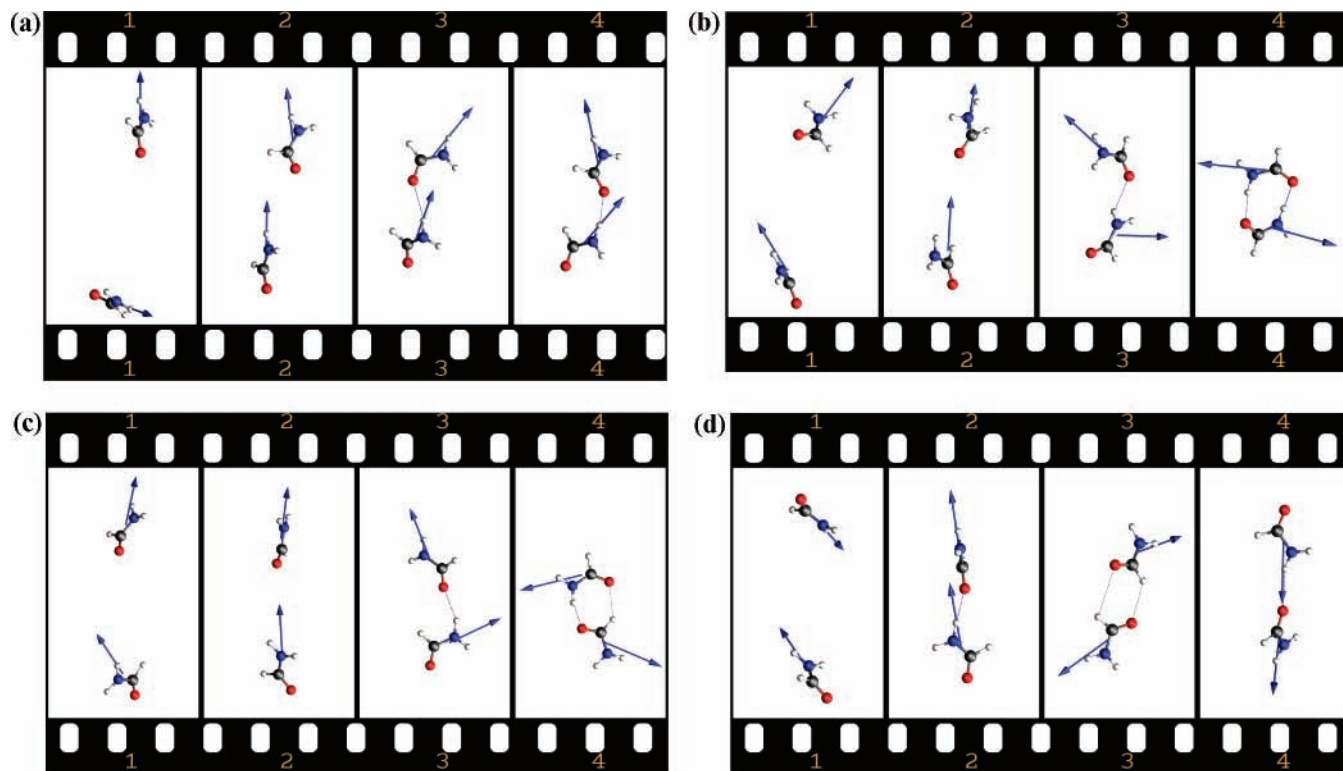
Formamide Dimers

J. Phys. Chem. A, Vol. 111, No. 42, 2007 **10559**

Figure 5. (a) Snapshots from a CP-MD simulation of the formation of structure **C/D** at 100 K. (1) $t = 0$: The two monomers are at the fixed C−C distance of 9.4 Å. (2) $t = 1.4$ ps: The monomers **M** are aligned along their dipole moments in the unconstrained run. (3) $t = 2.0$ ps: Dimer **C/D** configuration. (4) $t = 4.4$ ps: Structure **C/D** after internal rearrangement. Blue arrows indicate the calculated dipole moment for each FMA monomer at the selected step of the simulation. (b) Snapshots from a CP-MD simulation of the formation of dimer **A** at 100 K. (1) $t = 0$: The two monomers are at the fixed C−C distance of 9.4 Å. (2) $t = 0.8$ ps: The monomers are aligned along their dipole moments in the unconstrained run. (3) $t = 2.2$ ps: Formation of the structure **C/D**. (4) $t = 3.0$ ps: Final structure **A** after rearrangement. Blue arrows indicate the calculated dipole moment for each FMA monomer at the selected step of the simulation. (c) Snapshots from a CP-MD simulation of the formation of dimer **B** at 100 K. (1) $t = 0$: The two monomers are at the fixed C−C distance of 9.4 Å. (2) $t = 1.2$ ps: The monomers are aligned along their dipole moments in the unconstrained run. (3) $t = 2.2$ ps: Formation of the structure **C/D**. (4) $t = 3.0$ ps: Final structure **B** after rearrangement. Blue arrows indicate the calculated dipole moment for each FMA monomer at the selected step of the simulation. (d) Snapshots from a CP-MD simulation of the formation of structure **C/D** at 100 K. (1) $t = 0$: The two monomers are at the fixed C−C distance of 9.4 Å. (2) $t = 4.7$ ps: Formation of the structure **C/D**. (3) $t = 5.4$ ps: Formation of the structure **E** as an unstable intermediate state. (4) $t = 7.4$ ps: Structure **C/D** after rearrangement. Blue arrows indicate the calculated dipole moment for each FMA monomer at the selected step of the simulation.

respectively, dimer **A** having much higher intensity, though. Dimer **C/D** gives rise to rather broad spectra, which are probably hard to distinguish from spectral noise, in particular at low concentrations.

In the symmetric NH_2 spectral region (Figure 3d), a large red shift of 253 cm^{-1} is observed experimentally, which is comparable to that of the simulated spectra of dimers **A** and **B**. Although the position of the symmetric NH_2 stretch peak of dimer **B** predicted by the simulation is closer to the experimental band at 3158 cm^{-1}, its broadness makes it a less likely candidate than dimer **A**, which shows a sharp theoretical peak.

There are indications that the different matrix conditions, Ar and Xe, favor the formation of different dimer species. In the case Xe, the analysis of the spectral domains shown in Figure 3 suggests the predominance of complex **A**, with minor contributions of the **C/D** species. Signatures of complex **B** have been detected in the experimental spectra at 30 K when high FMA concentrations were deposited in the Xe matrix, but these signatures disappear during annealing as **B** rearranges to **A**.

Dimerization Simulations. Ab initio molecular dynamics simulations have been carried out of the aggregation of two formamide monomers. To mimic the conditions in the matrix isolation experiments, the simulations were carried out at a low temperature of 100 K. A slightly increased temperature is necessary in classical simulations to mimic quantum mechanical effects such as zero point motion. Moreover, a higher temper-

ature enhances the possibility of observing transitions between different local minimum structures on the relatively short time scale of the AIMD simulation. Following protocol 1 for a set of 20 different starting configurations (see the Computational Methods section for details), the monomers were initially kept apart for 10 ps by constraining the C−C distance in analogy to the low-temperature conditions in an argon matrix. During this phase, the monomers are seen to rotate at first and finally align according to their dipole moments (see snapshots 1 and 2 from Figures 5a−d), the C=O bond of monomer 1 pointing toward one of the N−H bonds of monomer 2, which is in the trans position with respect to the C=O bond.

Upon release of the distance constraint, the two monomers approach each other, and a C=O···H−N hydrogen bond is being formed. Subsequently, a rotation of the monomers about the newly formed hydrogen bond is observed, which corresponds to the superposition of structures **C** and **D** (Figure 5a, snapshot 3). Within the time period of 10−20 ps after release of the constraint, all of the trajectories were found to be in local minima structures **C** or **D**, frequently interconverting between the structures **C** and **D** (Figure 5a, snapshots 3 and 4). In this case, neither **A** nor **B** can be formed easily because of the repulsion between the hydrogen atoms of the N−H bond of monomer 1 and the C−H bond of monomer 2. In Table 7 the percentages of the different aggregation product species are listed. For protocol 1, we have 100% of dimer **C/D** and 0% of

TABLE 7: Statistical Data for the Occurrence of Different Types of the FMA Dimers A, B, C, D, and E after the Collision of Two FMA Monomer Molecules M

structure of the aggregation product	percentage		
	protocol 1: alignment	protocol 2: random	total
A	0%	13%	8%
B	0%	13%	8%
C/D	100%	74%	84%
E	0%	0%	0%

all other dimers. Please note that on the by many orders of magnitude longer time scale of the matrix isolation experiment structural rearrangement from **C/D** to either **A** or **B** cannot be excluded. On the contrary, it is highly likely that a large fraction of dimers will undergo a transition to a lower energy minimum structure.

In protocol 2 the two monomers were allowed to collide straightaway in an unconstrained run of about 10 ps without being previously aligned. Regardless of the initial configuration, in all aggregates the **C/D** dimer structure is formed initially due to dipole−dipole interaction. A single hydrogen bond is formed about which the monomers rotate, thus fluctuating between the **C** and the **D** local minima. For the majority of trajectories (74%, Table 7) during the time scale of the simulation no rearrangement to a more stable dimer form **A** or **B** was observed. However, for a fraction of 13%, we observe a rapid transformation from the singly hydrogen-bonded complex (dimer **C/D**) to the C_{2h} global minimum structure (dimer **A**, Figure 5b).

The formation of dimer **A** is triggered by the cleavage of the original C=O⋯H^{trans}−N hydrogen bond followed by the formation of a C=O⋯H^{cis}−N hydrogen bond. This rearrangement makes possible the formation of an additional hydrogen bond between the N−H group of monomer 1 and the C=O group of monomer 2, leading to the formation of dimer **A**.

In addition to the formation of dimer **A**, we have also observed the formation of dimer **B** for an equal number of simulations (13%, Table 7) within protocol 2. Figure 5c shows snapshots from a typical trajectory, illustrating the most important steps of the formation of dimer **B**. Similar to the mechanism leading to dimer **A**, the crucial steps are the breaking of the original C=O⋯H^{trans}−N hydrogen bond and the formation of a new C=O⋯H^{cis}−N hydrogen bond. This rearrangement enables interaction between the C−H group of monomer 1 and the C=O group of monomer 2, which leads to the formation of dimer **B**. Whereas the transition from **C/D** to structure **A** is very rapid (∼0.5 ps), the observed transformation to structure **B** is much slower (3−5 ps). Further transformation of **B** into **A** is not observed; dimer **B** remains stable for 10 ps.

The observed reaction pathways and outcomes for the two protocols differ very little qualitatively. Previous alignment of the system (protocol 1) clearly renders the formation of the superposition of structures **C** and **D** (Table 7) the most probable outcome. Protocol 2 allows for the formation of dimers **A** and **B** to a sizable degree; however, there is no evidence of the formation any other stable dimers such as dimer **E** (Figure 1), which is predicted to be energetically less favorable (Table 1). In one of our dimerization simulations temporary formation of **E** was observed serving only as an intermediate state in the transformation between **C** and **D** (Figure 5d).

We can only speculate which of the two protocols is the more realistic model to describe the matrix isolation experiment. It would seem probable that the ideal alignment of the monomer dipoles is somewhat disturbed by the rare gas matrix either

through steric effects or by collisions. Therefore our protocol 2, allowing for more randomness, may be the better representation.

To sum up the aggregation dynamics simulations, we observe that all reactions proceed via the initial formation of the **C/D** complex. In a fraction of collisions, rearrangement of **C/D** to dimers **A** or **B** is found to occur on the sub-picosecond time scale. It is clear that on the time scale of the experiment, at sufficiently high temperatures, there will be thermal transformation of **C/D** structures to the most stable structure **A**. However, we predict a high concentration of **C/D** complexes at very low temperatures, e.g., in superfluid liquid helium droplets.

Conclusion

The dimerization of FMA monomer **M** in argon matrixes leads to two products: the thermodynamically more stable dimer **A** with two strong N−H⋯O hydrogen bonds and the less stable **C/D** with only one strong hydrogen bond. In solid xenon evidence for an additional labile dimer **B** is found. A systematic computational study using the MMH method produces five dimers **A**−**E** that are minima at the MP2/cc-pVTZ level of theory. With a calculated dimerization energy of −10.4 kcal/mol **A** is, as expected, the most stable dimer found. In dimer **B** one of the FMA molecules is rotated in a way that a strong N−H⋯O interaction is replaced by a weaker C−H⋯O interaction, reducing the complex stabilization compared to **A** by about 4 kcal/mol. These two FMA dimers correspond to the two most stable dimers of formic acid, the well-known symmetrically bridged dimer **F** (corresponding to FMA dimer **A**) and the less stable asymmetrical dimer **G** (corresponding to FMA dimer **B**).[39,40] In the case of formic acid the less stable dimer **G** is primarily formed under conditions of matrix isolation but rearranges to the more stable dimer **F** on annealing the matrix. With FMA, dimer **B** is not observed after annealing, and instead the even less stable (−4.7 kcal/mol) dimer **C/D** is formed. Dimer **E** with a calculated dimerization energy of −2.9 kcal/mol is not observed in the experiment and, according to the ab initio molecular dynamics simulations, predicted to be unstable. The dynamics simulations also reveal that the structurally and energetically similar dimers **C** and **D** rapidly interconvert even at low temperatures. Thus, just three distinct dimers are remaining, **A**, **B**, and **C/D**, which are indeed observed in the experiment, **B** having been observed before annealing when high FMA concentrations had been deposited.

This leaves us with the question why besides the most stable dimer **A** only **C/D** but not **B** are formed during annealing of matrixes (both argon and xenon) containing **M**, whereas **B** is formed in small quantities after deposition of high concentrations of FMA in xenon. In contrast, annealing of matrixes containing the monomer of formic acid results in the formation of a dimer corresponding to **B** with one strong O−H⋯O and one weak C−H⋯O hydrogen bridge.[40] This formic acid dimer with further annealing rearranges to the more stable symmetrical dimer with two strong O−H⋯O hydrogen bridges (corresponding to FMA dimer **A**). The differences between formic acid and FMA are (i) the lower acidity of the N−H proton leading to less stable hydrogen bonds and (ii) the availability of two acidic NH hydrogen atoms in each FMA molecule (labeled cis and trans) increasing the structural possibilities for the formation of FMA dimers compared to formic acid dimers. In formic acid the cis conformer is the only conformer found after deposition in an inert gas matrix from the gas phase.

The formation of both dimers **A** and **C/D** in the argon matrix is a consequence of the first step of the dimerization of **M** in

which the carbonyl oxygen atom of one FMA molecule interacts with an amino hydrogen atom of the second molecule. There are two possible arrangements for this interaction leading to different dimers: (i) The cis hydrogen atom of the first FMA molecule interacts with the carbonyl oxygen atom of the second molecule. This can only lead to dimers **C** or **D**. (ii) The trans hydrogen atom of one FMA molecule interacts with the carbonyl oxygen atom of the second molecule leading to dimers **A** or **B**. The rearrangement of **C/D** to **A** or **B** requires breaking the strong N$-$H$_{cis}$···O hydrogen bond, which is energetically not possible under the conditions of matrix isolation. Thus, once one strong N$-$H···O hydrogen bond is formed, the further reaction leads to either **C/D** or **A/B**, which do not interconvert. In case ii obviously the energetically more stable complex **A** is formed rather than **B**.

cis H O
N
trans H H

cis H O
O
H
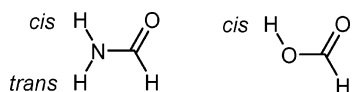
This simple picture is confirmed by the dynamics simulation. The initial alignment of the FMA monomers **M** occurs via long-range dipole$-$dipole interactions. This leads to an orientation of the two molecules **M** that preferentially produces **C/D** and less likely **A** or **B**. The activation barrier separating **A** from **B** is obviously not large enough to prevent the rearrangement of **B** to the thermodynamically more stable **A** under conditions of matrix isolation. Dimer **B** is therefore only formed if high concentrations of FMA are present, whereas annealing rapidly leads to rearrangement of dimer **B** to the thermodynamically more stable dimer **A**.

Supporting Information Available: Calculated frequencies of dimers **D** and **E**. This material is available free of charge via the Internet at http://pubs.acs.org.

References and Notes

(1) Vargas, R.; Garza, J.; Friesner, R. A.; Stern, H.; Hay, B. P.; Dixon, D. A. *J. Phys. Chem. A* **2001**, *105*, 4963.
(2) Cabaleiro-Lago, E. M.; Rios, M. A. *J. Chem. Phys.* **1999**, *110*, 6782.
(3) Hobza, P.; Havlas, Z. *Theor. Chem. Acc.* **1998**, *99*, 372.
(4) Bende, A.; Suhai, S. *Int. J. Quantum Chem.* **2005**, *103*, 841.
(5) Räsänen, M. *J. Mol. Struct.* **1983**, *101*, 275.
(6) Tsuchida, E. *J. Chem. Phys.* **2004**, *121*, 4740.
(7) Gomez Marigliano, A. C.; Varetti, E. L. *J. Phys. Chem. A* **2002**, *106*, 1100.
(8) Bende, A.; Vibok, A.; Halasz, G. J.; Suhai, S. *Int. J. Quantum Chem.* **2001**, *84*, 617.
(9) Papamokos, G. V.; Demetropoulos, I. N. *J. Phys. Chem. A* **2004**, *108*, 7291.
(10) Frey, J. A.; Leutwyler, S. *J. Phys. Chem. A* **2006**, *110*, 12512.
(11) Grabowski, S. J.; Sokalski, W. A.; Leszczynski, J. *J. Phys. Chem. A* **2006**, *110*, 4772.
(12) Lundell, J.; Krajewska, M.; Räsänen, M. *J. Phys. Chem. A* **1998**, *102*, 6643.
(13) King, S.-T. *J. Phys. Chem.* **1971**, *75*, 405.
(14) Fogarasi, G.; Szalay, P. G. *J. Phys. Chem. A* **1997**, *101*, 1400.
(15) Bukowska, J. *Pol. J. Chem.* **1981**, *55*, 879.
(16) Sanchez-Garcia, E.; Studentkowski, M.; Montero, L. A.; Sander, W. *ChemPhysChem.* **2005**, *6*, 618.
(17) Sanchez-Garcia, E.; George, L.; Montero, L. A.; Sander, W. *J. Phys. Chem. A* **2004**, *108*, 11846.
(18) George, L.; Sanchez-Garcia, E.; Sander, W. *J. Phys. Chem. A* **2003**, *107*, 6850.
(19) Sanchez-Garcia, E.; Mardyukov, A.; Studentkowski, M.; Montero, L. A.; Sander, W. *J. Phys. Chem. A* **2006**, *110*, 13775.
(20) Sanchez-Garcia, E.; Montero, L. A.; Sander, W. *J. Phys. Chem. A* **2006**, *110*, 12613.
(21) Montero, L. A.; Esteva, A. M.; Molina, J.; Zapardiel, A.; Hernandez, L.; Marquez, H.; Acosta, A. *J. Am. Chem. Soc.* **1998**, *120*, 12023.
(22) Montero, L. A.; Molina, J.; Fabian, J. *Int. J. Quantum Chem.* **2000**, *79*, 8.
(23) Dewar, M. J. S.; Zoebisch, E. G.; Healy, E. F.; Stewart, J. J. P. *J. Am. Chem. Soc.* **1985**, *107*, 3902.
(24) Stewart, J. J. P. *MOPAC*, version 6.0.
(25) Stewart, J. J. P. *J. Comput. Chem.* **1989**, *10*, 209.
(26) Stewart, J. J. P. *J. Comput.-Aided Mol. Des.* **1990**, *4*, 1.
(27) Moller, C.; Plesset, M. S. *Phys. Rev.* **1934**, *46*, 618.
(28) Frisch, M. J.; Pople, J. A.; Binkley, J. S. *J. Chem. Phys.* **1984**, *80*, 3265.
(29) Krishnan, R.; Binkley, J. S.; Seeger, R.; Pople, J. A. *J. Chem. Phys.* **1980**, *72*, 650.
(30) Dunning, T. H., Jr. *J. Chem. Phys.* **1989**, *90*, 1007.
(31) Frisch, M. J.; Trucks, G. W.; Schlegel, H. B.; Scuseria, G. E.; Robb, M. A.; Cheeseman, J. R.; Zakrzewski, V. G.; Montgomery, J. A., Jr.; Stratmann, R. E.; Burant, J. C.; Dapprich, S.; Millam, J. M.; Daniels, A. D.; Kudin, K. N.; Strain, M. C.; Farkas, O.; Tomasi, J.; Barone, V.; Cossi, M.; Cammi, R.; Mennucci, B.; Pomelli, C.; Adamo, C.; Clifford, S.; Ochterski, J.; Petersson, G. A.; Ayala, P. Y.; Cui, Q.; Morokuma, K.; Malick, D. K.; Rabuck, A. D.; Raghavachari, K.; Foresman, J. B.; Cioslowski, J.; Ortiz, J. V.; Stefanov, B. B.; Liu, G.; Liashenko, A.; Piskorz, P.; Komaromi, I.; Gomperts, R.; Martin, R. L.; Fox, D. J.; Keith, T.; Al-Laham, M. A.; Peng, C. Y.; Nanayakkara, A.; Gonzalez, C.; Challacombe, M.; Gill, P. M. W.; Johnson, B.; Chen, W.; Wong, M. W.; Andres, J. L.; Head-Gordon, M.; Replogle, E. S.; Pople, J. A. *Gaussian 98*, revision A.3; Gaussian, Inc.: Pittsburgh, PA, 1998.
(32) Frisch, M. J.; Trucks, G. W.; Schlegel, H. B.; Scuseria, G. E.; Robb, M. A.; Cheeseman, J. R.; Montgomery, J. A., Jr.; Vreven, T.; Kudin, K. N.; Burant, J. C.; Millam, J. M.; Iyengar, S. S.; Tomasi, J.; Barone, V.; Mennucci, B.; Cossi, M.; Scalmani, G.; Rega, N.; Petersson, G. A.; Nakatsuji, H.; Hada, M.; Ehara, M.; Toyota, K.; Fukuda, R.; Hasegawa, J.; Ishida, M.; Nakajima, T.; Honda, Y.; Kitao, O.; Nakai, H.; Klene, M.; Li, X.; Knox, J. E.; Hratchian, H. P.; Cross, J. B.; Bakken, V.; Adamo, C.; Jaramillo, J.; Gomperts, R.; Stratmann, R. E.; Yazyev, O.; Austin, A. J.; Cammi, R.; Pomelli, C.; Ochterski, J. W.; Ayala, P. Y.; Morokuma, K.; Voth, G. A.; Salvador, P.; Dannenberg, J. J.; Zakrzewski, V. G.; Dapprich, S.; Daniels, A. D.; Strain, M. C.; Farkas, O.; Malick, D. K.; Rabuck, A. D.; Raghavachari, K.; Foresman, J. B.; Ortiz, J. V.; Cui, Q.; Baboul, A. G.; Clifford, S.; Cioslowski, J.; Stefanov, B. B.; Liu, G.; Liashenko, A.; Piskorz, P.; Komaromi, I.; Martin, R. L.; Fox, D. J.; Keith, T.; Al-Laham, M. A.; Peng, C. Y.; Nanayakkara, A.; Challacombe, M.; Gill, P. M. W.; Johnson, B.; Chen, W.; Wong, M. W.; Gonzalez, C.; Pople, J. A. *Gaussian 03*, revision B.03; Gaussian, Inc.: Wallingford, CT, 2004.
(33) Boys, S. F.; Bernardi, F. *Mol. Phys.* **1970**, *19*, 553.
(34) Hutter, J. *CPMD*, version 3.10; MPI für Festkörperforschung: Stuttgart, Germany; IBM Zurich Research Laboratory: Zurich, Switzerland.
(35) Perdew, J. P.; Wang, Y. *Phys. Rev.* **1986**, 8800.
(36) Vanderbilt, D. *Phys. Rev. B* **1990**, *41*, 7892.
(37) Nose, S. *J. Chem. Phys.* **1984**, *81*, 511.
(38) Martinez, M.; Gaigeot, M. P.; Borgis, D.; Vuilleumier, R. *J. Chem. Phys.* **2006**, *125*, 144106.
(39) Halupka, M.; Sander, W. *Spectrochim. Acta, Part A* **1998**, *54A*, 495.
(40) Gantenberg, M.; Halupka, M.; Sander, W. *Chem.—Eur. J.* **2000**, *6*, 1865.